Journal of Nuclear Materials 393 (2009) 242–248

Contents lists available at ScienceDirect

Journal of Nuclear Materials

journal homepage: www.elsevier.com/locate/jnucmat

Characterization of oxide films formed on alloy 182 in simulated PWR primary water

J.-H. Liu [a,*], R. Mendonça [b,c], R.-W. Bosch [a], M.J. Konstantinović [a]

[a] Studiecentrum voor Kernenergie/Centre d'Etude de l'Energie Nucléaire (SCK·CEN), Boeretang 200, B-2400 Mol, Belgium
[b] CDTN, AV. Antonio Carlos 6627, Centro 31270901 Belo Horizonte, Brazil
[c] REDEMAT, Pç. Tiradentes 20, Centro 35400000 Ouro Preto, Brazil

ARTICLE INFO

Article history:
Received 20 January 2009
Accepted 11 June 2009

Keywords:
Alloy 182
Oxide film
SEM
Raman spectroscopy
XPS

ABSTRACT

The oxide film, formed on the alloy 182 due to the exposure to simulated Pressurized Water Reactor primary water conditions, is characterized using X-ray Photoelectron Spectroscopy, Scanning Electron Microscopy and Raman spectroscopy. As a consequence of the low redox potential for nickel, loosely bound oxide film consisting mainly of chromium oxide, is formed on the surface of the alloy. The oxide film is found to have a double-layer structure, with an inner layer rich in Cr_2O_3, outer layer rich in $FeCr_2O_4$. Thin $Ni(OH)_2$ and Fe_3O_4 clusters were observed on top of the oxide film. The morphology and thickness of the layers critically depend on the exposure times and surface treatments prior to the exposure.

1. Introduction

Primary water stress corrosion cracking (PWSCC) is known as one of the most important degradation phenomena which occurs in nickel-base alloys, exposed to harsh conditions of Pressurized Water Reactors (PWRs). For example, the PWSCC of alloy 600 is found in the primary side of actual PWRs [1]. In steam generators made of Ni-base alloys such as alloys 600 and 690, the properties of the oxide film formed due to exposure to the primary water of the PWR are argued to be crucial for the release of nickel in the coolant and stress corrosion cracking effects [2]. Previous studies of these alloys [2–6] showed that the oxide film has double-layer structure with an inner compact layer rich in chromium, and an outer layer consisting of well-defined octahedral Ni-rich crystals. A short-time experiment on alloys 690 and 600 in primary water conditions suggested a film structure with an internal layer of Cr_2O_3 and an external layer of $Ni(OH)_2$ [5]. It is also reported that the structure of the oxide layer of alloy 600 can be greatly influenced by dissolved hydrogen content in PWR primary water [1]. However, in spite of a detailed analysis, the reliable correlation between the characteristics of the oxide film and SCC effect is not yet fully established. In recent years, although significant field experience involving PWSCC has been observed on weld metal alloy 182 [7], the studies of oxide layer formed on it in PWR primary water conditions have not been reported. Therefore, we study the oxide layers formed on alloy 182 after exposure to simulated PWR primary water conditions.

Here we report the results of the oxide film characterization based on the X-ray Photoelectron Spectroscopy (XPS), Scanning Electron Microscopy (SEM) and Raman spectroscopy. The XPS was employed to study the chemical composition and thickness of the oxide film formed at different exposure times. The morphology of the oxide layers and the effects related to pre-treatments of the samples are analyzed by using SEM. The chemical structure of the oxide layer was obtained from the Raman scattering measurements.

2. Material

The material used in this study was commercial alloy 182. Its chemical composition is shown in Table 1. The exposure tests were carried out with cylindrical specimens (∅5 mm × 10 mm). In order to investigate the effects of surface roughness on the formation of the corrosion film, one surface of each cylinder was mechanically grinded, and the other was electro-polished for 10 s after mechanical grinding.

The prepared cylindrical specimens of alloy 182 were exposed to high temperature, high pressure water in a flowing (20 l/h) autoclave facility in the laboratory. The water chemistry in the autoclave was kept similar to the water chemistry of the PWR primary water (2 ppm Li, 1000 ppm B, 25 cc/kg H_2, 300 °C, 150 bar) used in a nuclear power plant. The exposure times were 1, 4 and 8 weeks.

* Corresponding author. Tel.: +32 (0)14 333181; fax: +32 (0)14 321216.
E-mail address: junhu.liu@sckcen.be (J.-H. Liu).

0022-3115/$ - see front matter © 2009 Elsevier B.V. All rights reserved.
doi:10.1016/j.jnucmat.2009.06.012

Table 1
The chemical composition of alloy 182.

Chemical composition, wt.%							
Fe	Cr	Mn	Ti	Nb	Ta	Si	Ni
9.9	14.7	6.7	0.33	1.07	0.022	0.5	bal.

3. Experiment

The exposed specimens were characterized using three techniques: the X-ray Photoelectron Spectroscopy (XPS: ESCALAB 220i-XL)/argon ion milling, the Scanning Electron Microscopy (SEM: JEOL 6310), and the Raman spectroscopy (Jobin Yvon T6400).

The oxide layer composition as a function of the thickness (depth) formed of each corrosion specimen was investigated by successively removing the surface material by argon ion bombardment coupled with XPS. In XPS, a monochromated X-ray source was used, consisting of a high power electron gun XR5, which provides Al Kα X-rays (energy of 1486.6 eV), with an energy spread of about 1 eV. The X-ray beam used for an analysis had a diameter of 500 μm. The pass energy of the energy analyzer was 100 eV and the step size was 0.2 eV. The 3 kV Ar^+ ions from an EXO5 ion source were employed for layer-by-layer erosion at a pressure of 4×10^{-8} mbar in the analysis chamber. The Ar^+ ion beam was incident at an angle of 45° and scanned for 100 s each time over an area of 2 mm × 2 mm. The ion current was around 1 μA. As a rough estimate, an etch rate of around 3 nm/min is assumed for the present sputtering conditions according to operating experiences [8–10].

The SEM was employed to characterize the gross features of the oxidized surface, including morphology of the outer layer of corrosion oxides. The Energy Dispersive X-ray Spectroscopy (EDS) attachment to the SEM probe was used to provide semi-quantitative estimation of surface oxide crystal compositions.

The Raman spectra were measured in a backscattering geometry using a Jobin Yvon T6400 spectrometer equipped with a LN_2 cooled charge coupled device camera. As an excitation source we used the 514.5 nm line from an Ar^+ laser. The beam with an average power of 5 mW was focused on the sample surface, which is kept under vacuum at room temperature. The measurement depth in the Raman spectroscopy is determined from the optical constant of the transition metal oxides. For example, in most of the Fe-, Cr- and Ni-oxides this depth is approximately 50 nm, 600 nm and 25 μm, respectively [11].

4. Results and discussion

4.1. Effect of pre-treatment on oxide film morphology

Fig. 1 shows SEM images of the surfaces of alloy 182 which were exposed to high temperature water for 8 weeks in the autoclave.

We found that the oxide film formed on the electro-polished surface, Fig. 1a and b, has different morphology from that formed

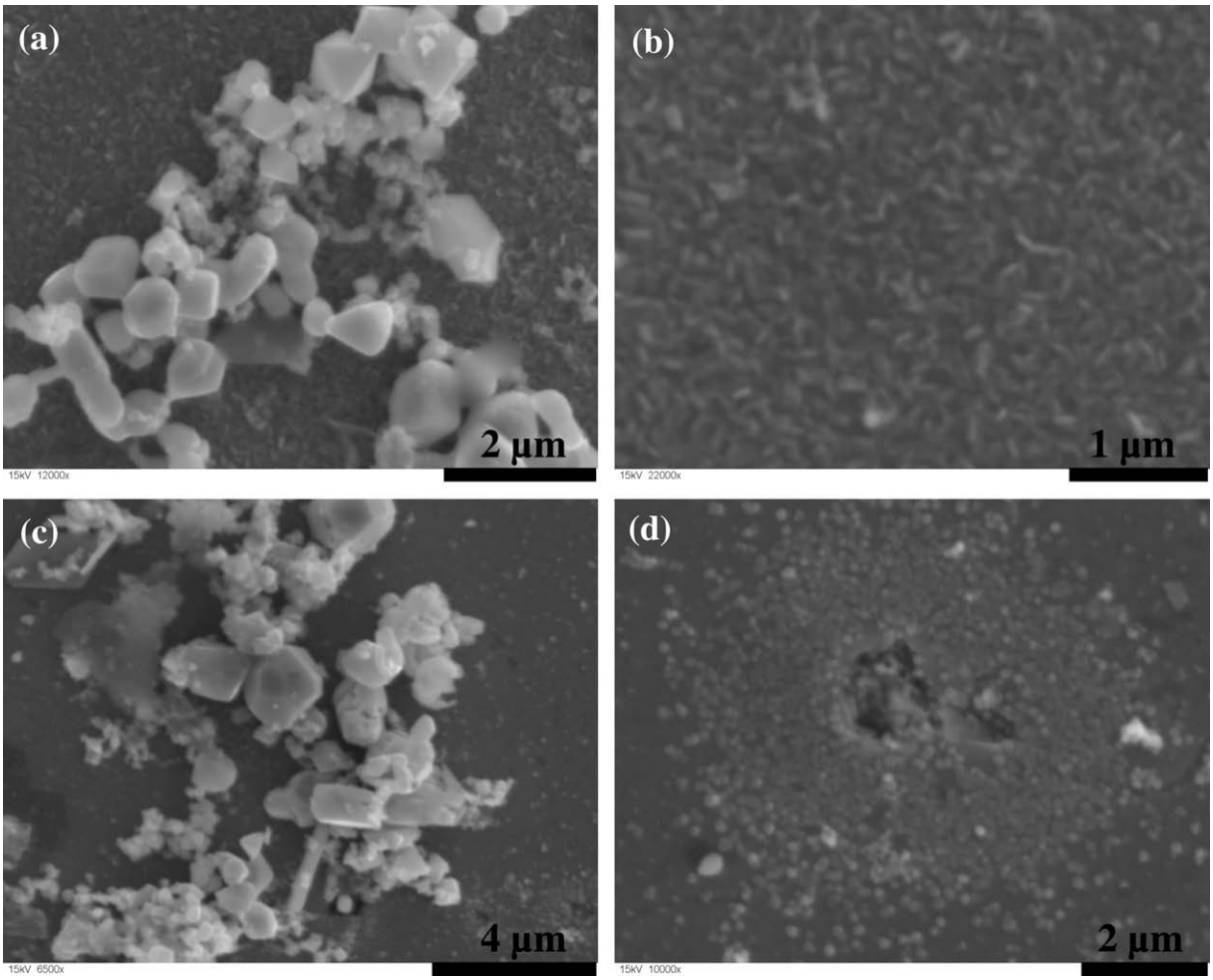

Fig. 1. SEM images of the alloy 182 after exposure for 8 weeks in the autoclave of (a) and (b) the electro-polished surface, (c) and (d) the mechanically grinded surface.

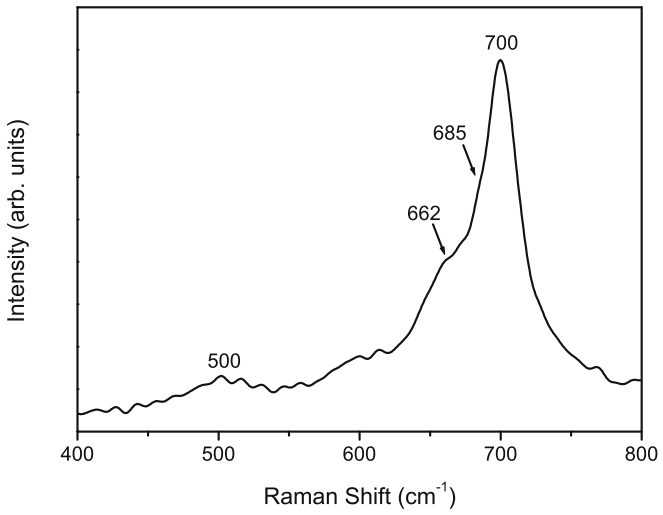

Fig. 2. Raman spectrum of electro-polished surface after 1 week exposure.

on mechanically grinded surface, Fig. 1c and d. In the former case, an exposure in high temperature water resulted in the formation of a uniform film consisting of small, needle-like crystals (0.25 μm long), see Fig. 1b. On top of this uniform film, larger clusters are deposited, see Fig. 1a. The EDS analyzes of these clusters revealed that they are rich in O and Fe, with presence of Cr, Ni and Nb. The uniform film contains more Ni and Cr, and less Fe and O than the big clusters. However, it is important to underline that the EDS spectra are also influenced by the signal from base metal, since the thickness of the oxide film is typically around ~200 nm.

On the other hand, the exposure of mechanically grinded surface did not result in the formation of uniform film. Instead, many corrosion pits are observed on the surface. Fig. 1d shows one typical pit, with many small particles around it. The EDS analyzes revealed the presence of Nb and Mn in these particles. The clusters found on the mechanically ground surface after exposure, Fig. 1c, have a similar composition to those observed in Fig. 1a. Different morphologies shown in Fig. 1b and d originate from different surface quality before the exposure, since surface quality often has a marked effect on the pitting resistance. In the present work, the electro-polished surface is smoother than the mechanically grinded surface. Because of that, the pitting and localized corrosion are less likely to occur on electro-polished surface [12], leading to homogeneous corrosion and formation of uniform oxide film. On the contrary, the mechanically ground surface was locally corroded and pitted.

4.2. Raman spectrum of the oxide film

The Raman spectrum of the electro-polished surface after 1 week exposure is shown in Fig. 2. The strongest peak at about 700 cm^{-1} and its shoulder peak at 662 cm^{-1} can be assigned either to $NiFe_2O_4$ or to Fe_3O_4 crystals [13,14]. However, as it will be discussed later, Ni is present through the oxide layer as metallic Ni so we attribute these two peaks to Fe_3O_4. The additional peak at 685 cm^{-1} and the weak broad peak at around 500 cm^{-1} are assigned to $FeCr_2O_4$ [11,13,15].

4.3. The XPS study of the oxide film

4.3.1. Qualitative evaluation of XPS spectra

For both the mechanically grinded and electro-polished surfaces the oxide film thickness is found to be different depending on the exposure time. The chemical states of the alloy elements in the oxide film change in a similar way. Because of that, the electro-polished surface after 1 week exposure is taken as the reference for the qualitative evaluation of the XPS spectra.

4.3.1.1. Ni2p spectra. Fig. 3 shows the Ni2p XPS spectra. At the specimen surface before sputtering (0 s sputtering time), Ni2p spectrum consists of the intense peak (peak 1), corresponding to $2p_{3/2}$ state at the binding energy of 855.9 eV, and its satellite peak (peak 2) at about 862.1 eV. The C 1s is at 285.0 eV. According to the literature data [16], these two features originate from $Ni(OH)_2$. Besides, an additional low intensity peak (peak 1′) at about 852.3 eV is clearly visible on the lower binding energy side of peak 1. This peak gains intensity after removing the $Ni(OH)_2$ and becomes the most dominant peak after 100 s sputtering. Its satellite peak (peak 2′) appears at 858.3 eV. The spectra collected after longer sputtering times ($\geqslant$200 s) have similar features, indicating no further change of the single chemical state. Moreover, the intensity ratio between the satellite and main $Ni2p_{3/2}$ photoelectron peak is less than 0.20. By comparing these data with published data on Ni2p in Ni [16], NiO [16], $NiFe_2O_4$ [17], $NiCr_2O_4$ [17] and $NiFe_xCr_{2-x}O_4$ (x = 0.5, 1.0 and 1.5) [17], we found that the observed chemical state of Ni characterized by peaks 1′, 2′, 3′ and 4′ corresponds to metallic Ni. Here, one has to be cautious of interpreting depth profiling of Ni oxide by ion bombardment: NiO is very susceptible to reduction by ion bombardment during XPS profiling, which can reduce NiO to metallic Ni because of preferential sputtering of oxygen. However, the produced Ni^0 peak is just a shoulder peak of the dominant/main peak for the oxide, as confirmed by Oswald [18]. In our study, after 100 s sputtering, the dominant peak in the $Ni2p_{3/2}$ region is $Ni^0 2p_{3/2}$ peak. When $Ni(OH)_2$ is completely removed ($\geqslant$200 s sputtering), pure spectra for metallic Ni is obtained. Furthermore, even before sputtering the spectrum (0 s in Fig. 3) already shows the presence of metallic Ni. This is indicated by the weak $Ni^0 2p_{3/2}$ peak (peak 1′) which is visible on the low binding energy side of $Ni^{2+}2p_{3/2}$ (peak 1) in $Ni(OH)_2$. Thus, we believe that the presence of metallic Ni is not due to the preferential sputtering of oxygen from Ni-oxides. Instead, Ni was not oxidized during exposure test.

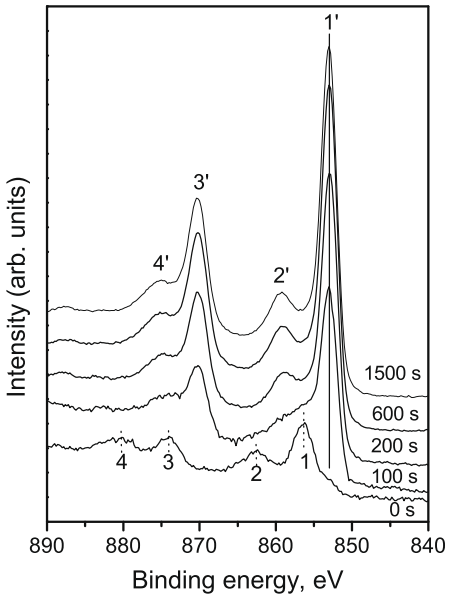

Fig. 3. The Ni2p XPS spectra taken from the electro-polished surface after 1 week exposure. The peaks denoted as 1, 2, 3, 4, and 1′, 2′, 3′, 4′, correspond to $Ni2p_{3/2}$, satellite of $Ni2p_{3/2}$, $Ni2p_{1/2}$, and satellite of $Ni2p_{1/2}$, of $Ni(OH)_2$ and metallic Ni, respectively.

Therefore, Ni is present in the sample surface with a single chemical state, corresponding to Ni^0 or metallic Ni, except for a 5 nm thin $Ni(OH)_2$ layer (the electro-polished surface after 1 week exposure) on the top of the surface. The XPS measurements of electro-polished alloy 182 before exposure also revealed the existence of a thin $Ni(OH)_2$ layer. Thus, $Ni(OH)_2$ is formed on the sample surface as a result of the reaction of Ni with water vapor in air. The fact that Ni was not corroded (oxidized) in the presence of PWR primary water environment can be explained on the basis of the corrosion potential [1,19,20]. The corrosion potential of Ni in PWR water at 300 °C is close to the equilibrium potential of the Ni/NiO transition due to the large amount of dissolved hydrogen. In the present simulated PWR primary water conditions, the potential was lower than the transition potential, so Ni is thermodynamically stable and should remain in the metallic state Ni^0 [21].

Since Ni, as the major alloy element, was not oxidized during exposure, the formed oxide film is mainly composed of Cr–Fe–O system oxide. The role of other minor components (Mn, Nb, Ti, Si) in the oxide layer has been ignored in the present study. With respect to the Cr–Fe–O system corrosion oxide, Ignatova [9] showed that Ar^+ sputtering in XPS depth profiling introduced only very little preferential sputtering. The XPS measurement of Ignatova was performed at SCK·CEN. We have used the same instrument in the present work. The sputtering conditions in both works are very similar.

4.3.1.2. Cr2p spectra. The Cr2p XPS spectra are shown in Fig. 4. Chromium initially appears in a completely oxidized state as Cr^{3+}, since the binding energy of $Cr2p_{3/2}$ is found to be 576.6 eV. After 200 s sputtering, a new peak starts to appear at the binding energy of 573.6 eV. Further sputtering gradually removes the Cr^{3+} oxide component. Finally, only peak at 573.6 eV remains, corresponding to metallic chromium in the unoxidized base metal.

4.3.1.3. Fe2p spectra. In general, the identification of iron chemical states is more difficult, since iron may exist in different valence states as well as in mixed valence, with the chemical shifts close to each other. The analysis of the XPS spectra of Fe^{3+} (in Fe_2O_3), and Fe^{2+} (in Fe_2SiO_4) ions [22] have shown that the binding energies of $Fe^{3+}2p_{3/2}$ and $Fe^{2+}2p_{3/2}$ are 711.0 eV and 709.0 eV, respectively. However, the binding energy of $Fe2p_{3/2}$ in Fe_3O_4 is 710.6 eV [22], which is in between the values obtained for Fe^{2+} and Fe^{3+}. Moreover, nickel, as the major alloy element in alloy 182, has a strong Auger peak in the vicinity of $Fe2p_{3/2}$ (for both Fe_2O_3 and Fe_3O_4) when using Al anode in XPS, which makes the identification of iron chemical states based on the chemical shift of $2p_{3/2}$ more difficult. In this study, the identification of iron chemical states relies on the satellite peaks of $Fe2p_{3/2}$, and the peak position of $Fe2p_{1/2}$. Typically, the satellite peak of $Fe^{3+}2p_{3/2}$ is located at approximately 8 eV higher than the main $Fe2p_{3/2}$ peak, at 718.8 eV. The satellite peak of $Fe^{2+}2p_{3/2}$ is located approximately 6 eV higher than the main $Fe2p_{3/2}$ peak, at about 715.5 eV. It has been reported that $Fe2p_{3/2}$ state of Fe_3O_4 at about 724.0 eV [22], does not have a satellite peak [22–24].

The Fe2p XPS spectra are shown in Fig. 5. The longer sputtering times ($\geqslant$300 s) does not change the spectra. Besides the strong Ni-Auger peak, two main peaks for $Fe2p_{3/2}$ (peak 1) and $Fe2p_{1/2}$ (peak 2) appear at 706.8 eV and 719.8 eV, respectively, which is indication of metallic iron. Before sputtering, $Fe2p_{1/2}$ peak position is found to be 723.8 eV (peak 3′). No satellite peak was found. This indicates the presence of Fe_3O_4 on the sample surface, which is in accordance with the Raman measurement. Typically, Fe_3O_4 is formed as a deposit on the surface, as already discussed and shown in Fig. 1. The spectrum after 100 s sputtering revealed new oxidation state at 722.7 eV for $Fe2p_{1/2}$ (peak 3) and the satellite peak of $Fe2p_{3/2}$ (peak 4) at 715.2 eV. This is characteristic of Fe^{2+} state in the form of $FeCr_2O_4$. The oxidized iron is completely removed after 200 s sputtering. By comparing the XPS spectra of Fe2p and Cr2p, Figs. 5 and 4, we observed that it takes more sputtering time to completely remove oxidized chromium than to remove oxidized iron.

4.3.1.4. Nb3d and Mn3p spectra. Fig. 6 presents the Nb3d XPS spectra. It is found that Nb initially occurs in completely oxidized state, as Nb^{4+}, since the peak positions of $Nb3d_{5/2}$ (peak 2) and $Nb3d_{3/2}$ (peak 2′) are at 206.3 eV and 209.0 eV, respectively. After 100 s sputtering time, the new components (peaks 1 and 1′) start to appear. Further sputtering, up to 700 s, gradually removes Nb^{4+}, and only the new component is visible in the spectra. The binding energies of peak 1 and peak 1′ are 202.3 eV and 205.0 eV, respectively. They correspond to metallic niobium.

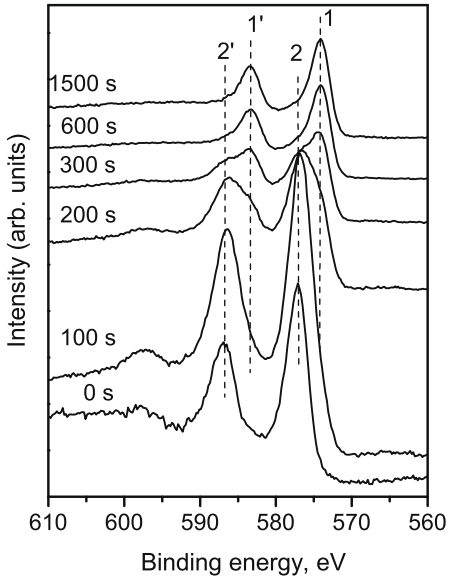

Fig. 4. Cr2p XPS spectra of electro-polished surface after 1 week exposure. The peaks donated as 1, 1′, 2 and 2′ correspond to $Cr^0 2p_{3/2}$, $Cr^0 2p_{1/2}$, $Cr^{3+}2p_{3/2}$ and $Cr^{3+}2p_{1/2}$, respectively.

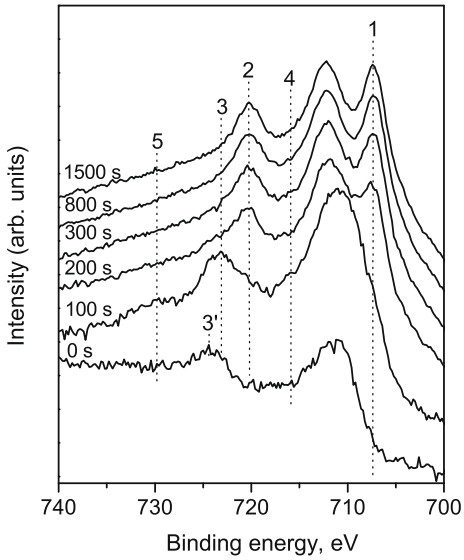

Fig. 5. Fe2p XPS spectra of electro-polished surface after 1 week exposure. The peaks donated as 1, 2, 3, 3′, 4 and 5 correspond to $Fe^0 2p_{3/2}$, $Fe^0 2p_{1/2}$, $Fe^{2+}2p_{1/2}$, $Fe2p_{1/2}$ of Fe_3O_4, satellite of $Fe2p_{3/2}$ and satellite of $Fe2p_{1/2}$, respectively.

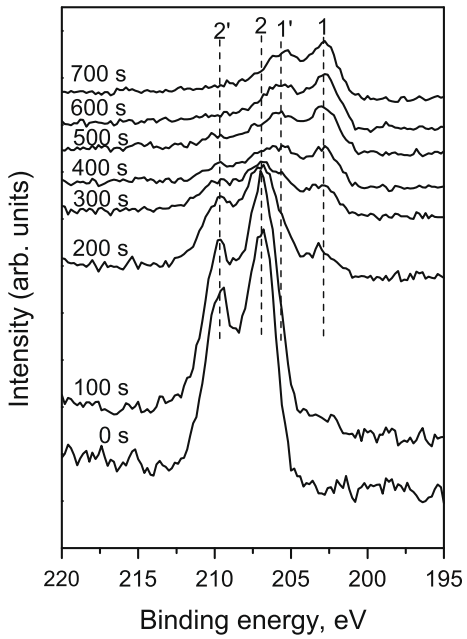

Fig. 6. Nb3d XPS spectra of electro-polished surface after 1 week exposure. The peaks donated as 1, 1′, 2 and 2′ correspond to $Nb^0 3d_{5/2}$, $Nb^0 3d_{3/2}$, $Nb^{4+} 3d_{5/2}$ and $Nb^{4+} 3d_{3/2}$, respectively.

Due to the fact that Ni-Auger peak overlaps with $Mn2p_{3/2}$ peak, Mn3p peak was taken for the evaluation of the manganese chemical state. Initially, manganese also appears in completely oxidized state. After 100 s sputtering a new component starts to increase in intensity. The sputtering up to 700 s gradually removes the oxidized state, and only the new component was left in the spectra. The sputtering up to 1500 s does not change the shape of the Mn3p peak. Therefore, this new component at 46.4 eV, should correspond to metallic manganese in the unoxidized base metal. The binding energy of the oxidized component, Mn^{n+}, is at about 47.5 eV. Therefore, Mn exists in the oxide layer as oxide.

4.3.2. The XPS depth profile of the oxide film

The depth profiles of all analyzed surfaces are similar, except for the oxide film thickness which can be estimated on the basis of the sputtering rate discussed in the experimental paragraph. Since niobium and manganese contents in the oxide layer are below 2 at%, only depth profiles of the main elements, nickel, chromium, iron and oxygen, are discussed. Fig. 7 shows the elemental depth profile of the electro-polished surface after exposure for three different times, 1, 4, and 8 weeks. Since Ni is present throughout the 'oxide film' as metallic Ni, a pure dense oxide film does not exist. Therefore, we use the term 'oxidation affected layer' instead of the 'oxide film'. The oxide film in the 'oxidation affected layer' consists of Cr, Fe and O. As discussed in Section 4.3.1, Fe and Cr exist in the 'oxidation affected layer' as Fe^{2+} and Cr^{3+}. Furthermore, it is found that it takes more time to remove Cr^{3+} than to remove Fe^{2+}. This indicates that the 'oxidation affected layer' has a double-layer structure. In the outer layer Fe^{2+} and Cr^{3+} co-exist in $FeCr_2O_4$. However, in the inner layer the oxide ion is Cr^{3+}, most probably in the form Cr_2O_3. Therefore, the 'oxidation affected layer' can be defined as a layer in which Cr^{3+} could be found. The thickness of this layer can be estimated from the depth profile of Cr^{3+}, which is shown in Fig. 8. The sputtering times needed to completely remove Cr^{3+} are 800 s, 1400 s and >3000 s for the electro-polished surface after exposure for 1 week, 4 weeks and 8 weeks, respectively. Multiplying the sputtering time by sputtering rate of 3 nm/min, the thickness of 'oxidation affected layer' for these three exposure times can be estimated, namely 40 nm, 70 nm and >150 nm, respectively. By comparing Figs. 7 and 8, one can also

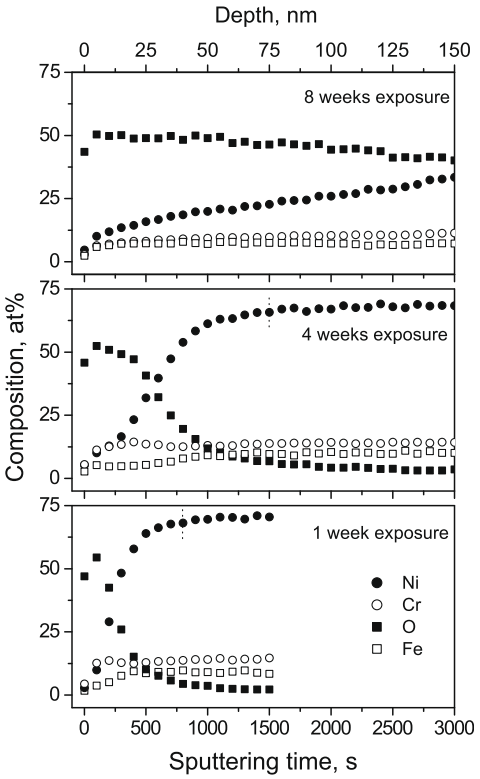

Fig. 7. Depth profile of the electro-polished surface after exposure for 1 week, 4 weeks and 8 weeks.

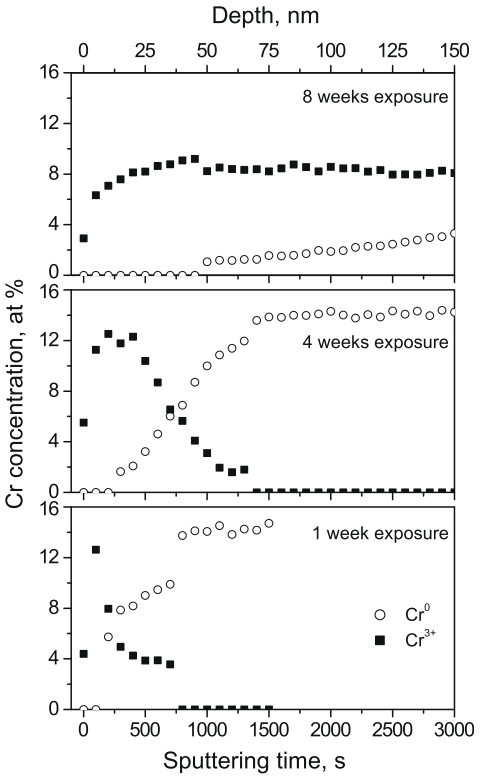

Fig. 8. Depth profile of Cr^0/Cr^{3+} for the electro-polished surface after exposure for 1 week, 4 weeks and 8 weeks.

find that the complete removal of Cr^{3+} is accompanied with Ni reaching the plateau value.

As previously mentioned, the 'oxidation affected layer' has a double-layer structure. In the outer layer Fe^{2+} and Cr^{3+} co-exist in $FeCr_2O_4$. The inner layer is formed by Cr_2O_3. This is confirmed by observing the depth profile of Cr^0 and Cr^{3+} for the sample exposed to PWR primary water for 4 weeks, see Fig. 8. As one can see, the Cr^{3+} concentration has a constant value until around 400 s sputtering time. Up to that point, the Fe concentration (see Fig. 7 for 4 weeks exposure) has constant value too, and the chemical state of Fe is Fe^{2+}. Accordingly, the outer layer should be rich with $FeCr_2O_4$. After removal of $FeCr_2O_4$ layer, metallic Fe is revealed, and Cr appears in two forms: Cr^{3+} in Cr_2O_3 and metallic Cr.

Due to lack of pure dense oxide film formation, the 'oxidation affected layer', especially the outer layer, is loosely bond to the substrate. This is confirmed by measuring the XPS spectra of the surface cleaned with soft pencil eraser. After eraser cleaning, the specimen surface was cleaned with acetone in ultra-sonic bath to remove contamination by eraser. Elemental depth profiles of eraser cleaned surface are shown in Figs. 9 and 10. Both Figures indicate that eraser cleaning reduced the thickness of the 'oxidation affected layer' from 70 nm to about 35 nm. The Ni concentration reaches a plateau value at this thickness. Moreover, after eraser cleaning the chemical state of Fe is found to be Fe^0. This proves that $FeCr_2O_4$ is completely removed by eraser, and that only Cr_2O_3 remains on the surface (Mn and Nb are ignored in this study).

Finally let us discuss the effect of surface pre-treatments. Even though the XPS depth profile of mechanically grinded surfaces have similar behaviour as for electro-polished surfaces, the estimated thickness of 'oxidation affected layer' on the mechanically grinded surfaces are not consistent with the exposure times. The 'oxidation affected layers' are thicker for the 1 week and 4 week exposures of the mechanically grinded surfaces in comparison with electro-polished surfaces. However, vice versa is found for the 8 weeks exposed samples. This effect occurs due to different surface roughnesses. In is interesting to note that although different surface pre-treatments resulted in very different oxide morphologies, see Fig. 1, the XPS depth profiles are found to be very similar.

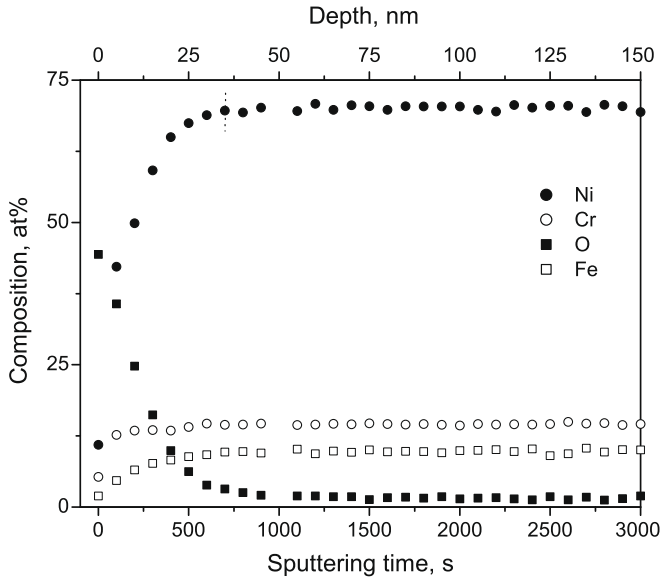

Fig. 9. Depth profile of the electro-polished surface after exposure for 4 weeks and eraser cleaning.

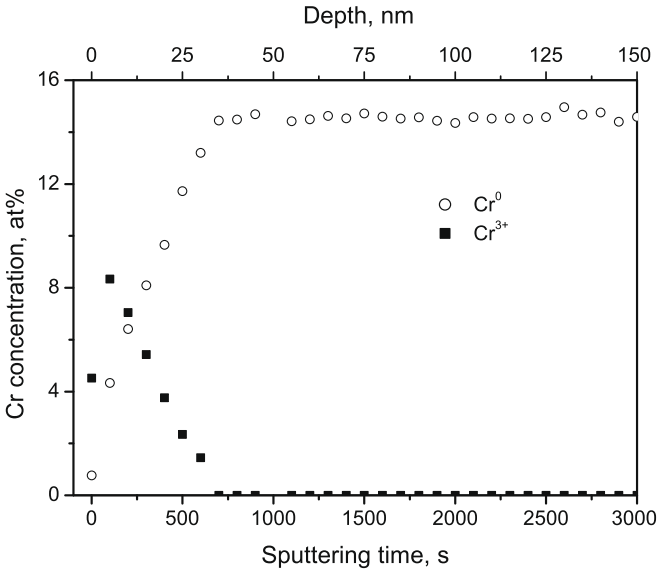

Fig. 10. Depth profile of Cr^0/Cr^{3+} for the electro-polished surface after exposure for 4 weeks and eraser cleaning.

5. Conclusions

We characterized the oxide films formed on alloy 182 in simulated PWR primary water using SEM-EDS, Raman spectroscopy and XPS. The main conclusions are:

(1) SEM-EDS results showed that sample pre-treatment has remarkable effect on the formation of the oxide film. A uniform oxide film rich in nickel was formed on the electro-polished surface. However, the corrosion pits rich in Nb and Mn were observed on the grinded surface. Both surfaces showed the presence of clusters rich in Fe and O.
(2) Raman spectroscopy and XPS measurements revealed the presence of Fe_3O_4 and $FeCr_2O_4$. The former is probably a deposit from the water.
(3) The XPS measurements showed that the major alloy element Ni was not corroded, except for a thin $Ni(OH)_2$ layer on the top of the surface. Other alloying elements, Cr, Fe, Nb and Mn, showed the transition from the oxidized states to metallic states. Since Ni was not corroded during exposure, no pure dense oxide film was formed during the exposure. Because of that an 'oxidation affected layer' was introduced. The thickness of this 'oxidation affected layer' can be estimated on the basis of Cr^{3+} XPS profiles. Longer exposure time results in a thicker 'oxidation affected layer' on the electro-polished surfaces. No consistent results were obtained in that respect for the mechanically grinded surfaces due to non-controlled surface roughness.
(4) The XPS measurements revealed a double-layer structure of the 'oxidation affected layer'. The outer layer is rich in $FeCr_2O_4$, and the inner layer formed by Cr_2O_3.
(5) The 'oxidation affected layer', especially the outer layer, is loosely bonded to the surface, and can be easily removed by a soft pencil eraser.

Acknowledgements

This work is partly supported by the GDF Suez-SCK·CEN 2008-2012 convention. Part of the work has been sponsored by the bilateral cooperation Belgium–Brazil SPO 2005-2008 with contract

number BL/52/BR01. We thank Dr. Z. Dohčević for the measurements of the Raman spectra.

References

[1] T. Terachi, N. Totsuka, T. Yamada, T. Nakagawa, H. Deguchi, M. Horiuchi, M. Oshitani, J. Nucl. Sci. Technol. 40 (2003) 509–516.
[2] L. Marchetti, S. Perrin, O. Raquet, F. Miserque, M. Pijolat, F. Valdivieso, Y. Wouters, in: Fontevrand 2006, Fontevrand, France, September 18–22, 2006.
[3] F. Carrette, M.C. Lafont, G. Chatainier, L. Guinard, B. Pieraggi, Surf. Interf. Anal. 34 (2002) 135–138.
[4] A. Machet, A. Galtayries, P. Marcus, P. Combrade, P. Jolivet, P. Scott, Surf. Interf. Anal. 34 (2002) 197–200.
[5] A. Machet, A. Galtayries, S. Zanna, L. Klein, V. Maurice, P. Jolivet, M. Foucault, P. Combrade, P. Scott, P. Marcus, Electrochim. Acta 49 (2004) 3957–3964.
[6] J. Panter, B. Viguier, J.M. Cloue, M. Foucault, P. Combrade, E. Andrieu, J. Nucl. Mater. 348 (2006) 213–221.
[7] F. Vaillant, J.M. Boursier, C. Amzallag, C. Bibollet, S. Pons, Les Materiaux Dans Le Nucleaire (2007) 62–71.
[8] Thermo Electron Corporation, Ex05 ion gun system operating manual, issue 1, 2003.
[9] V.A. Ignatova, S. Van Dyck, R. Grotzschel, W. Moller, Surf. Interf. Anal. 38 (2006) 396–400.
[10] V.A. Ignatova, S. Van Dyck, S. Gavrilov, M. Vankeerberghen, Internal Project Report (PERFECT: F16O-CT-2003-508840), SCK·CEN, 2006.
[11] R.L. Farrow, R.E. Benner, A.S. Nagelberg, P.L. Mattern, Thin Solid Films 73 (1980) 353–358.
[12] M.G. Fontana, in: Sanjeev Rao (Ed.), Corrosion Engineering, third ed., McGraw-Hill, Inc., 1986, ISBN 0-07-100360-6.
[13] M. Da Cunha Belo, M. Waals, N.E. Hakiki, J. Corset, E. Picquenard, G. Sagon, D. Noel, Corros. Sci. 40 (1998) 447–463.
[14] P.R. Graves, C. Johnston, J.J. Campaniello, Mater. Res. Bull. 23 (1988) 1651–1660.
[15] S.C. Tjong, Mater. Res. Bull. 18 (1983) 157–165.
[16] H.W. Nisbitt, D. Legrand, G.M. Bancroft, Phys. Chem. Miner. 27 (2000) 357–366.
[17] G.C. Allen, S.J. Harris, J.A. Jutson, Appl. Surf. Sci. 37 (1989) 111–134.
[18] S. Oswald, W. Brückner, Surf. Interf. Anal. 36 (2004) 17–22.
[19] T. Nakagawa, N. Totsuka, T. Terachi, N. Nakajima, J. Nucl. Sci. Technol. 40 (2003) 39–43.
[20] E. Schuster, K.H. Neeb, W. Ahlfänger, R. Henkelmann, R.T.J. ärnström, J. Nucl. Mater. 152 (1988) 1–8.
[21] D.S. Morton, S.A. Attanasio, J.S. Fish, M.K. Schurman, in: CORROSION 1999, San Antonio, Texas, USA, April 25–30, 1999.
[22] T. Yamashita, P. hayes, Appl. Surf. Sci. 254 (2008) 2441–2449.
[23] D.D. Hawn, B.M. DeKoven, Surf. Interf. Anal. 10 (1987) 63–74.
[24] M. Muhler, R. Sehiogl, G. Ertl, J. Catal. 138 (1992) 413–444.